

# Scorch arisen prediction through elastomer flow in extrusion die

J. Launay · N. Allanic · P. Mousseau · R. Muller ·  
R. Deterre

Received: 17 July 2012 / Accepted: 4 December 2012 / Published online: 18 December 2012  
© Springer-Verlag France 2012

**Abstract** The thermal and kinetic behaviour of an elastomer flow inside an extrusion die is numerically investigated. The aim is to control scorch arisen and reduce the heating time in the mould by using viscous dissipation phenomena in order to improve the rubber compound curing efficiency. A three dimensional model, using the particle tracking technique, is developed in order to get thermal, velocity and kinetic fields through the flow. Three common geometries of an elastomer forming process are modeled: a straight runner, a bend zone and a bifurcation. This simulation is applied on the case of an EPDM (ethylene propylene diene monomer) flow. The thermal and rheological properties are experimentally characterized. The influence of viscous dissipation on the reaction progress of the melt is studied on several process conditions. Many criterions relevant for thermal and cure homogeneity are proposed in order to quantify the performance of geometry modifications.

**Keywords** Elastomer moulding process · Viscous dissipation · Scorch · Particle tracking · Ansys Polyflow

## Introduction

The viscous dissipation within molten polymers flow leads to a heating. Brinkman [1] was the first to determine that the rise of temperature mainly occurs near the wall making the temperature profile inhomogeneous. In order to understand viscous heating implication on polymer flows, many numerical and experimental studies were performed in relation with industrial processes. Karkri et al. [2] measured temperatures

along a rectangular extrusion die as an entry of an inverse method, to determine the thermal state of the extruded melt. By this way, they showed the importance of viscous dissipation on the heat transfer occurring in the polymer flow. Pujos et al. [3] performed a similar study with measurements in unsteady flow, experimenting injection moulding conditions. Another numerical and experimental study involving viscous dissipation in a heat exchanger was performed by Yataghene et al. [4], with good agreement between both determinations. In this study, thermal profiles inside the exchanger were described with particular interest on the viscous dissipation. This phenomenon is also of a great interest concerning the rheometrical characterization due to its influence in capillary flow. For example, Laun [5] proposed a technique in order to treat the Bagley curves taking into account the viscous dissipation, when Kang et al. [6] developed a numerical analysis procedure to correct the influence of viscous heating on slip parameters determined from capillary data.

In the case of rubbers, due to their high viscosity and pronounced pseudoplastic behaviour, the local changes of temperature are amplified. As an example, during their study on automobile weather strip extrusion, Ha et al. [7] found temperature differences varying between 10 and 40 °C in a 6 cm extrusion head with a thickness of 1 cm. During forming processes, like extrusion or injection moulding, it could lead to the premature vulcanization of the fluid, currently named “scorch”. The flow inside processes could be blocked involving an important waste of time in the industry production, of material and machinery degradation. To avoid this phenomenon, industrials currently modify their elastomer formulation. By changing the quantity of inhibitors in their blend, they have the possibility to avoid scorch arisen and control elastomer curing [7]. However, the reactivity of the elastomer depends on its thermal history and a heterogeneous temperature distribution leads to a heterogeneous reaction progress in material. This point can be the origin of material degradation in the mold. Thus, an important issue is to obtain a homogeneous thermal and kinetic material at the mold inlet.

J. Launay (✉) · N. Allanic · P. Mousseau · R. Deterre  
CNRS, GEPEA, UMR 6144, IUT de Nantes, LUNAM Université,  
Université de Nantes, 2 avenue du Professeur Jean Rouxel,  
44475 Carquefou Cédex, France  
e-mail: julien.launay@univ-nantes.fr

R. Muller  
ECPM Strasbourg, LIPHT, FRE2711, Strasbourg, France

Even if the physicochemical (e.g. change of composition) method is often used to control curing efficiency, it has a weak influence on thermal and kinetic homogeneity of the material.

This work focuses on the influence of the runners design on the thermal and kinetic profiles of the material [8–10] and thus on scorch arisen. In this way, the present study reports the numerical comparison of three kinds of runners usually found in forming processes like extrusion or injection molding. The aim is to model the thermal, rheological and kinetic behaviour of rubber inside an extrusion die in order to determine the influence of viscous heating on the reaction progress of the melt. Thus, a model based on energy balance and Navier–Stokes equations was investigated to calculate the thermal, pressure and velocity fields. Then, so as to determine the reaction progress of the melt during the flow, a particle tracking technique was set up, based on the knowledge of the thermal history. Using this heat generation could help reducing the curing time during forming processes, and, with an adequate redistribution of the melt, it would become possible to get homogeneous thermal and kinetic profiles. Thereby, to analyze behavior of elastomer flow, several performance criterions are defined. They are used in order to check the thermal and curing distribution in the various studied geometries. Finally, a sensitivity analysis of material and process parameters is performed.

**Problem description**

**Equations**

As previously considered by Alok et al. [11] during their numerical study of the extrusion forming process, we consider the rubber flow as an incompressible non-newtonian material, and the process steady-state. Due to the high viscosity of this kind of material, and knowing in practice that mean velocity of polymer melt flow in forming process is around 0.1 m.s<sup>-1</sup>, the Reynolds number is currently lower than 0.1 [12]. Thus, the viscous forces dominate in the momentum equation balance and inertial effects are negligible as well. The gravitational effects can also be neglected. The computational model consists in one domain corresponding to the material flow as

illustrated on Fig. 1. Thus, the non-isothermal and laminar rubber flow as previously considered during studies of rubber extrusion [13] is described by the governing equations [14]:

$$\vec{\nabla} \cdot \vec{V} = 0 \tag{1}$$

$$\rho(\vec{V} \cdot \vec{\nabla}) \cdot \vec{V} = -\vec{\nabla} p + \vec{\nabla} \cdot \left[ \eta \left( \vec{\nabla} \vec{V} + \vec{\nabla}^T \vec{V} \right) \right] \tag{2}$$

$$\rho C_p (\vec{V} \cdot \vec{\nabla}) T = \vec{\nabla} \cdot (\lambda \vec{\nabla} T) + \Phi \tag{3}$$

where  $\vec{V}$  is the velocity of the fluid,  $p$  the pressure,  $\rho$  the density,  $C_p$  the heat capacity and  $\lambda$  the thermal conductivity.

The viscous dissipation  $\Phi$  is expressed by:

$$\Phi = \eta \dot{\gamma}^2 \tag{4}$$

with  $\eta$  the viscosity and  $\dot{\gamma}$  the shear-rate

Concerning the boundary conditions, previous studies on the wall slippage of rubber shown that under a shear stress value at the wall, no slip was observed [15]. In our case, we study the flow of rubber in runners of 10 mm diameter, involving low shear stresses at the wall. As a first approach, a no-slip condition is also assumed. At the inlet, a constant radial temperature profile is imposed. The boundary conditions are given as follows:

$$\Gamma_{in} : p = p_{in}; \frac{\partial \vec{V}}{\partial \vec{n}} = 0; T = T_{in} \tag{5}$$

$$\Gamma_{out} : p = p_0; \frac{\partial \vec{V}}{\partial \vec{n}} = 0; \frac{\partial T}{\partial \vec{n}} = \vec{0}; \tag{6}$$

$$\Gamma_L : \vec{V} = \vec{0}; T = T_L \tag{7}$$

$\vec{n}$  is the outgoing unit normal vector,  $p_0$  the atmospheric pressure,  $\Gamma_{in}$  denotes the inlet surface,  $\Gamma_{out}$  the outlet surface and  $\Gamma_L$  the surface in contact with the extruder barrel as represented on Fig. 1.

The induction period, which prevents any vulcanization reaction, notably described by Rafei et al. [16], is considered

**Fig. 1** Geometry modification through elastomer flow

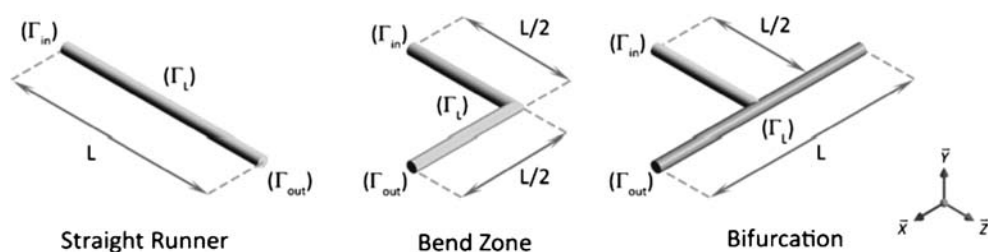


**Table 1** Thermophysical properties of elastomer

Thermal properties	Units	Values
$\rho$ (20 °C)	kg.m <sup>-3</sup>	1086
$\lambda$ (20 °C)	W.m <sup>-1</sup> .K <sup>-1</sup>	0.309
$C_p$ (150 °C)	J.kg <sup>-1</sup> .K <sup>-1</sup>	1912
Viscosity parameters		
$K_0$	Pa.s <sup>n</sup>	29 300
$E_a$	J.mol <sup>-1</sup>	814
$K$ (150 °C)	Pa.s <sup>n</sup>	56230
$n$		0.193
Induction time constants		
$t_0$ (150 °C)	s	4,06 10 <sup>-3</sup>
$E$	J.mol <sup>-1</sup>	31072
$R$	J.mol <sup>-1</sup> .K <sup>-1</sup>	8.314

by introducing the induction time  $\beta$ . Thus the scorch arisen corresponds to the start of elastomer curing ( $\beta=1$ ). Claxton and Liska [17] suggested an Arrhenius law to calculate the reaction progress in an isothermal case (Eq. 8), modified by Isayev and Deng [18] to take into account the thermal history of the material (Eq. 9):

$$t_i = t_0(T_0) \exp\left(\frac{E_{ai}}{R} \left(\frac{1}{T} - \frac{1}{T_0}\right)\right) \tag{8}$$

$$\beta = \int_0^t \frac{1}{t_i(T)} \tag{9}$$

with  $R$  the ideal gas constant,  $E_{ai}$  the activation energy, characteristic of the material and  $t_0(T_0)$  the induction time at the reference temperature  $T_0$ :

$$t_0(T_0) = \exp\left(\frac{E_{ai}}{RT_0}\right) \tag{10}$$

Materials and methods

The numerical study is performed in the case of an elastomer EPDM (ethylene propylene diene monomer) flow, particularly prone to viscous heating due to its highly pseudoplastic behaviour. The thermal and kinetic properties of the blend are given in Table 1. The thermal conductivity was measured at 20 °C by Hot Disk TPS 2500 [19] and thermal capacity was determined by differential scanning calorimetry analysis from 40 to 180 °C [20]. A mechanical analysis was performed by using a moving die rheometer in order to characterize the kinetic reaction [21, 22]. A fitting procedure was then applied to experimental results in order to estimate kinetic parameters  $t_0$  and  $E_{ai}$ .

The rheological characterization of material is given on Fig. 2. It was characterized with a Rosand capillary rheometer RH2000 (Malvern) for shear rates from 25 s<sup>-1</sup> to 10<sup>4</sup> s<sup>-1</sup>, and temperatures from 100 to 160 °C [23]. Several capillaries of 1 mm diameter and different lengths were used in order to apply the Bagley correction [24]. Results take also into account Rabinowitsch correction [25].

In this first numerical approach, the elongational flow through studied geometries is not taken into account and a shear flow is considered [26]. In this way, the pseudo-plastic behaviour of the fluid is described by the following power-law model as previously used in other studies [27]:

$$\eta(T, \dot{\gamma}) = K(T_0) \cdot \exp\left(\frac{E_a}{R} \left(\frac{1}{T} - \frac{1}{T_0}\right)\right) \dot{\gamma}^{n-1} \tag{11}$$

**Fig. 2** Viscosity versus shear rate

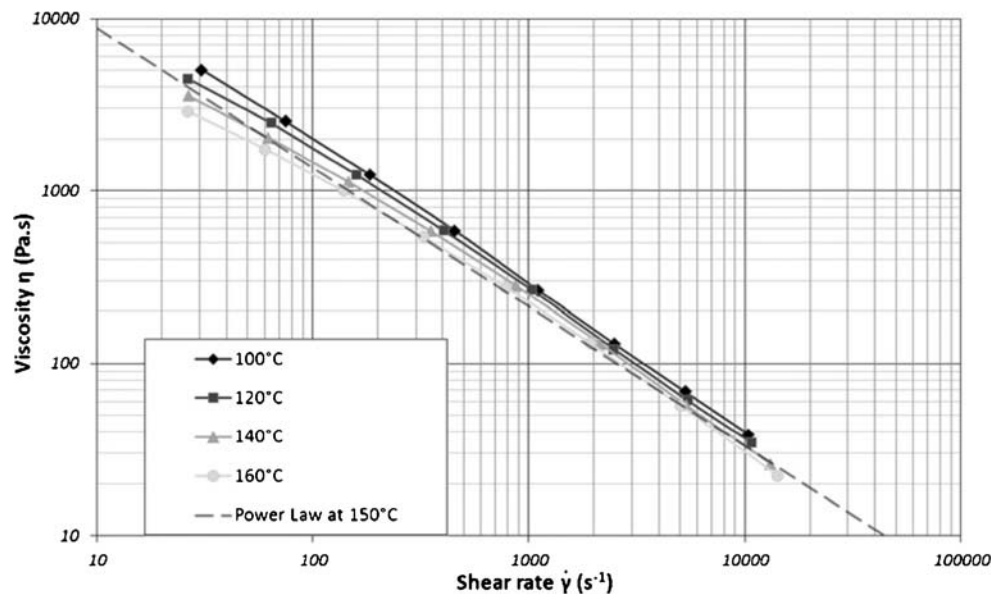
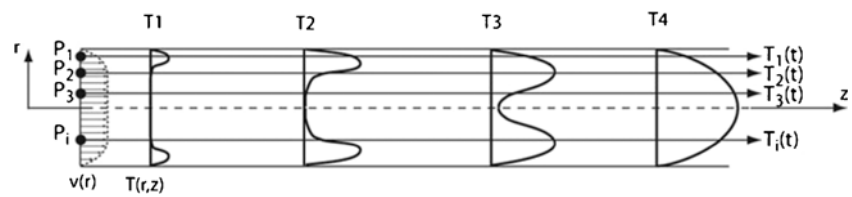


**Fig. 3** Particle tracking technique principle



$$K(T_0) = K_0 \exp\left(\frac{E_a}{RT_0}\right) \quad (12)$$

The consistency factor  $K$ , the activation energy  $E_a$  and the power-law index  $n$ , determined by fitting the shear viscosity, are given in Table 1. The dependence of viscosity with temperature is described by an Arrhenius law as it is currently made in literature [28]. Thus, with the retained viscosity model, the mean relative error between predicted and experimental viscosity is 8 %. As an example, the modelled viscosity obtained for  $T=T_0=150$  °C is plotted on Fig. 2. The comparison with experimental data obtained at 140 °C and 160 °C shows the weak influence of temperature on viscosity. Thus, to limit numerical difficulties, the elastomer rheological behaviour is simplified in the model and described as follows:

$$\eta(\dot{\gamma}) = K(T_0) \cdot \dot{\gamma}^{n-1} \quad (13)$$

#### Numerical procedure

The finite element model is built with the Ansys Polyflow software [28]. Three geometries are studied: a straight runner, a bend zone and a bifurcation (Fig. 1). All geometries were reduced for symmetry's sake: in axisymmetric coordinates in the case of the straight runner, in 3D half geometry for the bend zone and in 3D quarter geometry for the bifurcation.

The solving of Eqs. (1) to (6) is done by using a direct method based on Gaussian elimination. In our study, the studied viscous fluid having a power-law index lower than 0.7, the Picard iterative scheme is used instead of Newton–Raphson iterations in order to provide a better convergence [29].

Then, based on thermal behaviour of elastomer, a particle tracking technique, known as mixing simulation in Ansys Polyflow is investigated in order to calculate the reaction progress. Connelly and Kokini [30] used a similar numerical approach to study the mixing in single and twins screw mixers. The methodology retained is presented on Fig. 3 for a cylindrical runner. Many rubber material points are initially randomly distributed through the input section. The residence time and particles flow paths are determined from the velocity field using a fourth order Runge–Kutta scheme. Knowing the successive spatial positions of particles, the thermal history is recovered from the thermal field. As an example, this evolution is schemed for the cylindrical runner, in the hypothesis of a same temperature at the wall and on the inlet, on Fig. 3. At the beginning ( $T_1$ ), viscous heating is responsible for a rise of temperature near the wall where the velocity gradients are highest. A part of energy generated by viscous dissipation is lost through the extruder barrel, whereas the other part still contributes to the rising of the temperature near the wall ( $T_2$ ). Temperature gradients become significant between edge and center of the flow, dissipated energy will then be conducted towards the center of the flow, making its temperature increases ( $T_3$ ). Finally,

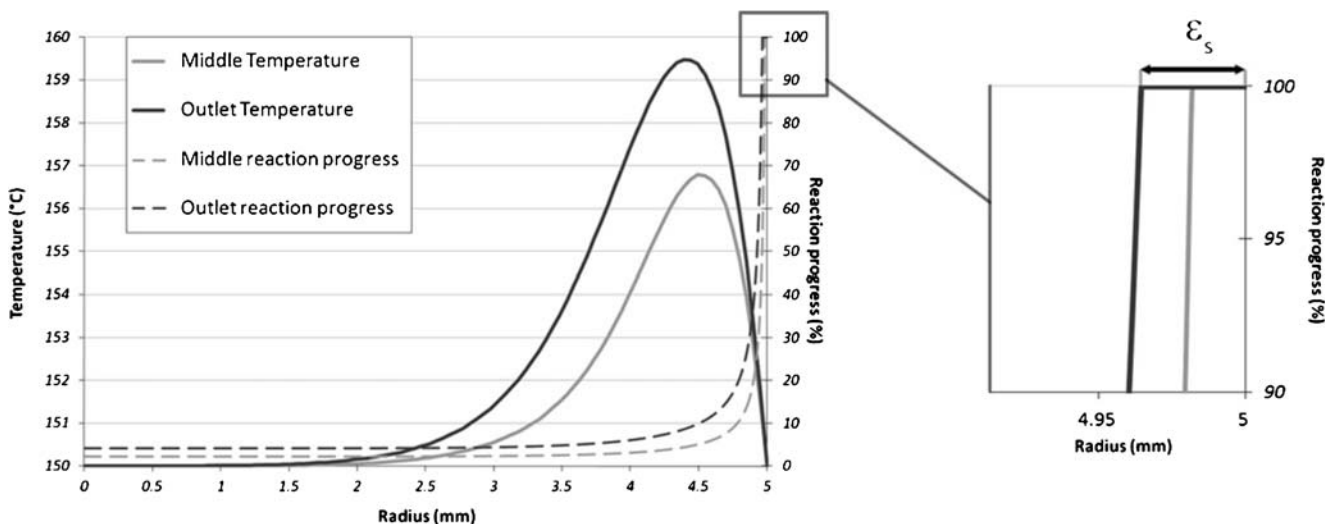


**Fig. 4** Thermal and kinetic profiles in a straight runner obtained with  $Q=10^{-5} \text{ m}^3 \cdot \text{s}^{-1}$  and  $T_{in}=T_L=150$  °C

**Table 2** Results of numerical simulations obtained for a cylindrical runner ( $T_{in}=T_1=150\text{ }^\circ\text{C}$ )

$Q$ ( $10^{-5}\text{ m}^3\cdot\text{s}^{-1}$ )	$\Delta p$ (MPa)	$\dot{\gamma}_w$ ( $\text{s}^{-1}$ )	$\Phi$ (W)	$\Phi_L$ (W)	$T_{out}$ ( $^\circ\text{C}$ )	$\sigma_T$ ( $^\circ\text{C}$ )	$\beta_{out}$ (%)	$\sigma_\beta$ (%)	$\varepsilon_s$ ( $\mu\text{m}$ )	$\alpha_s$	$I_\beta$
0.5	11.1	102.2	55.2	30.3	152.3	2	13.3	14.2	72	0.4	0.94
1	12.6	204.5	126.2	59.3	153.1	3.2	7.25	10.9	35	0.2	0.66
2	14.5	408.9	288.6	114.4	154.1	4.9	3.96	8.0	17.5	0.1	0.48
3	15.6	613.4	468.1	166.8	154.8	6.2	2.68	6.17	3	0.06	0.44

after a sufficient length, a stationary profile is developed, with equality between energy lost through the extruder barrel and the energy conserved in the material ( $T_4$ ). Then, the reaction progress through stream lines is deduced of thermal history by using Eqs. (7) and (8). A sensibility study on the particle tracking parameters was performed so as to have an acceptable calculation time while keeping quality of results. In order to deduce the residence time of particles inside the runner of the velocity fields, an integration time of  $5\text{ }\mu\text{s}$  is used. Moreover, due to calculation problem involved by material particles having velocity tending to zero, a limit on residence time is fixed to 500 s. 500 particles are launched in the straight runner; numerical uncertainties on induction time are also lower than  $10^{-4}$ . In the 3D model cases, 5000 particles are necessary to obtain a similar quality of results.

**Results and discussion**

For numerical tests, the straight runner, the bend zone and the bifurcation, are considered having an equivalent neutral fiber flow length of  $L=200\text{ mm}$  (dotted lines in Fig. 1) and a 10 mm nominal diameter. Considering an usual upper extrusion temperature limit for elastomer extrusion of  $150\text{ }^\circ\text{C}$ , simulations are carried with an extruder barrel temperature and initial flow temperature equals to this reference temperature ( $T_{in}=T_L=T_0=150\text{ }^\circ\text{C}$ ). Such a temperature allows us to study scorch arisen in the most critical extrusion case. At the inlet, reaction of the elastomer was assumed to have not yet begun ( $\beta=0$ ). The high pseudo-plastic behavior of

elastomer implies higher velocity gradients in the vicinity of the wall. To get better accuracy, inflation was applied on the mesh layers of all geometries. In the following numerical tests, a growth factor of 1.1 starting from the wall is applied with a minimum radial layer thickness of  $5\cdot 10^{-5}\text{ m}$  for the straight runner, and  $10^{-4}$  for the two other cases. A  $5\cdot 10^{-4}\text{ m}$  length is applied on the mesh in the flow direction.

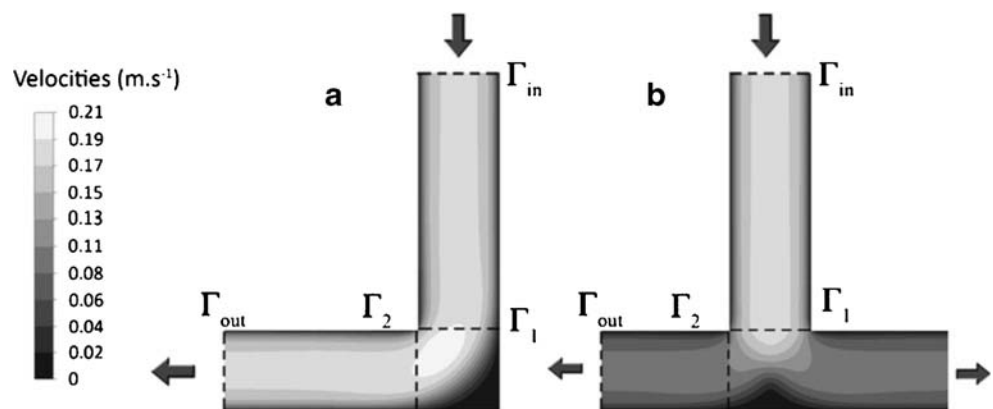
After performing an analysis of scorch arisen of the elastomer flow in a straight runner, the comparison of the three geometries modifications are carried out on velocities, temperatures and kinetic profiles of the flow.

**Study of straight runner**

Figure 4 shows numerical results obtained for the straight runner elastomer flow taken as a reference geometry. A fixed volume flowrate  $Q=10^{-5}\text{ m}^3\text{ s}^{-1}$  was considered. The profiles of temperature are given, so as the reaction progress, at the middle ( $z=100\text{ mm}$ ) and outlet positions. In the studied case, the center of the flow remains unheated like in the second case  $T_2$  represented on Fig. 3. The temperature profiles show a rise near the wall where velocity gradients are maximal. At the middle of the runner, the maximal temperature is  $156.8\text{ }^\circ\text{C}$  and is of 2.7 K greater at the outlet. All along the runner, the rise of temperature tends to expand towards the center of the flow, which still remains at the inlet temperature.

The reaction progress highly depends on residence time, and is also maximal near the wall, where velocity tends to zero. When the velocity becomes lower than  $0.5\text{ mm}\cdot\text{s}^{-1}$ ,

**Fig. 5** Velocity fields in the bend zone (a) and in the bifurcation (b) geometries near to the change of direction



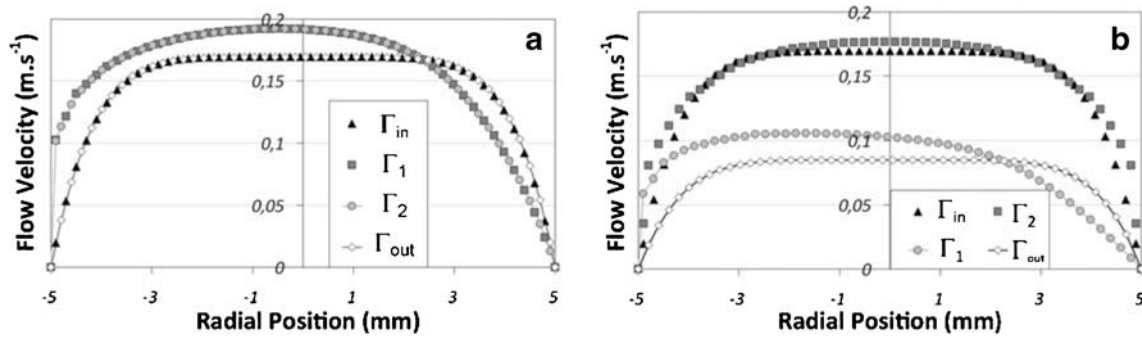


Fig. 6 Flow velocities profile in bend zone (a) and bifurcation (b)

particles are assumed to be stagnant. Thus, we define a rate of material's stagnation  $\alpha_s$  as follows:

$$\alpha_s = \frac{V_s}{V} \quad (14)$$

where  $V_s$  is the stagnated material volume and  $V$  is the geometry volume.

In the studied case,  $\alpha_s=0.4\%$ , which confirms that in this reference geometry, a relatively low material mass is immobilized all along the flow. Besides, due to the no-slip hypothesis applied on the boundary layer, the performed simulations present a scorch thickness  $\varepsilon_s=35\ \mu\text{m}$ , represented on Fig. 4, where all the material present a reaction progress  $\beta=1$ .

In a second time, numerical simulations are performed by considering volume flowrates variation between  $0.5 \times 10^{-5}\ \text{m}^3 \cdot \text{s}^{-1}$  and  $3 \times 10^{-5}\ \text{m}^3 \cdot \text{s}^{-1}$ , corresponding to a variation of pressure ( $\Delta P$ ) from 11.1 MPa to 15.6 MPa. All the results characterizing the elastomer flow are presented in Table 2. The heat generated by viscous dissipation all along the runner ( $\Phi$ ), the maximal shear rate obtained close to the wall ( $\dot{\gamma}_m$ ), and the thermal power exchanged with the extruder barrel ( $\Phi_L$ ) are given. Concerning the outlet section, the bulk temperature ( $T_{out}$ ) [31] and the mean reaction progress ( $\beta_{out}$ ) are given. As a comparison with these both parameters, we also calculate ( $\sigma_\beta$ ) and ( $\sigma_T$ ), which are the

standard deviations of reaction progress  $\beta$  and temperature distribution respectively, versus radius.

The results given in Table 2 show that the increasing of the flow rate and thus shear rates enable the heat generated by viscous dissipation to be enhanced, and thus to get a higher outlet temperature. The maximum shear rate in the flow increases linearly with the flow rate. At  $Q=3 \times 10^{-5}\ \text{m}^3 \cdot \text{s}^{-1}$ , the maximal shear rate reaches  $613.4\ \text{s}^{-1}$ . Thus, in this configuration the viscosity decreases to 316.4 Pa.s. An important viscous dissipation in the flow is involved and the corresponding mean rise of temperature of 4.8 K becomes significant. Due to localized overheating, the material is thermally less homogeneous ( $\sigma_T=6.2\ \text{°C}$ ). In parallel, we can note that thermal exchanges with the extruder barrel are important. At low flow rate, it represents 55 % of the thermal power generated, then it diminishes with increasing flow rate. However, at  $Q=3 \times 10^{-5}\ \text{m}^3 \cdot \text{s}^{-1}$ , it still represents 36 % of the heat generated by viscous dissipation. Moreover, increase the flowrate enables the material's stagnation to be avoided, its rate decreases towards  $\alpha_s=0.06\%$ .

To obtain a curing homogeneity inside the mould, the melt profile would be ideally homogenized in temperature and in reaction progress. Moreover, by considering the possible energy saving inside the mould, the reaction progress should be close to one at the end of the flow. In the studied cases, the kinetic behaviour is principally influenced

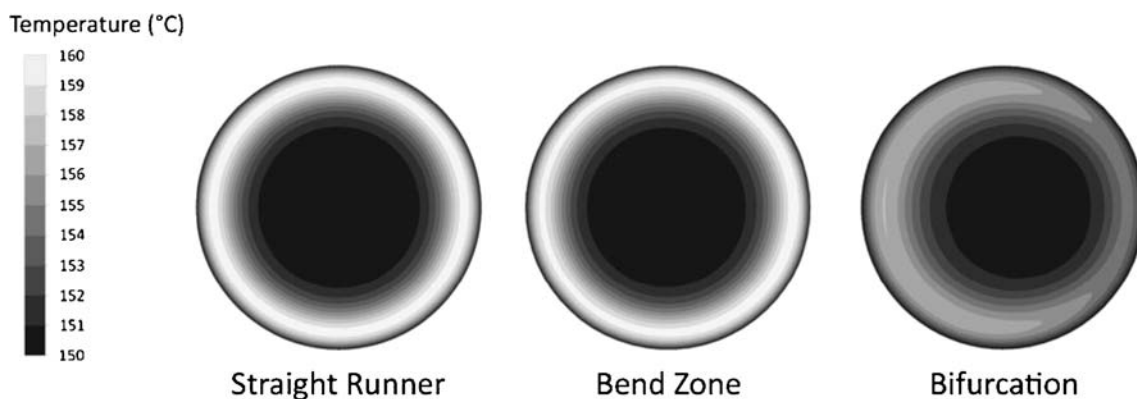


Fig. 7 Temperature profiles in the outlet surface

**Table 3** Results of numerical simulations obtained for several geometries with  $Q=10^{-5} \text{ m}^3 \cdot \text{s}^{-1}$  and  $T_{\text{in}}=T_1=150 \text{ }^\circ\text{C}$ 

Geometry	$\Delta P$ (MPa)	$\Phi$ (W)	$\Phi_w$ (W)	$T_{\text{out}}$ ( $^\circ\text{C}$ )	$\sigma_T$ ( $^\circ\text{C}$ )	$\beta_{\text{out}}$ (%)	$\sigma_\beta$ (%)	$\alpha_s$ (%)	$I_\beta$
Straight runner	12.6	126.2	59.3	153.1	3.2	7.2	10.8	0.2	0.66
Bend zone	12.6	125.9	54.7	154.2	3.2	7.8	9.4	1.8	0.82
Bifurcation	11.7	117.3	56	153.5	1.9	11.4	14	2.4	0.81

by the residence time inside the geometry. At lowest flow rate, the mean reaction progress reaches  $\beta_{\text{out}}=13.3 \%$ . However, the elastomer kinetic state is very heterogeneous ( $\sigma_\beta=14.2 \%$ ) and the scorch thickness is highest ( $\varepsilon_s=75 \mu\text{m}$ ).

Thus, to determine the ability of geometry to reach an ideal state, we introduce a kinetic performance index  $I_\beta$  defined as follows:

$$I_\beta = \frac{\beta_{\text{out}}}{\sigma_\beta} \quad (15)$$

Through this criterion, the compromise between the global reaction progress and the kinetic homogeneity is described. For instance, the kinetic performance factor stays close for the two highest flow rates, what indicates a similar elastomer kinetic state at the outlet.

#### Influence of geometry changes on thermal and kinetic behavior flow

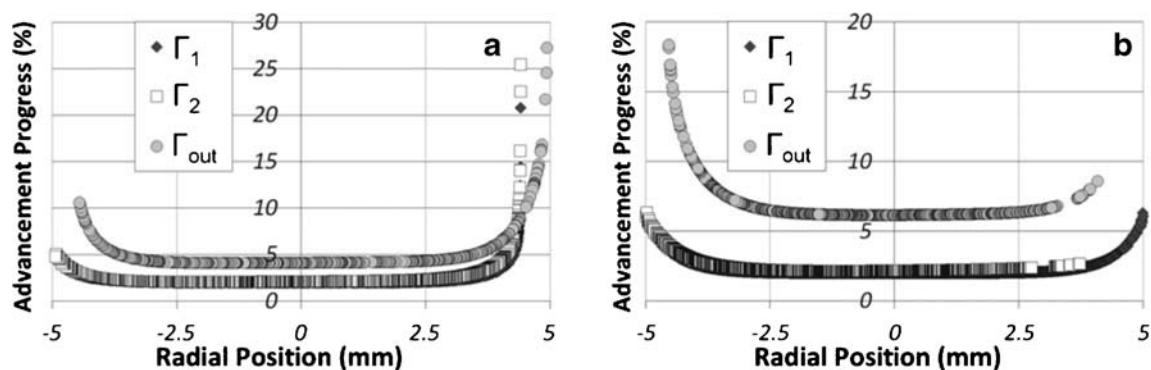
In this section, the influence of the modification of the geometry on the elastomer flow is discussed. Numerical results obtained for a bend zone and a bifurcation are compared to previous results described for a straight runner, by considering a constant volume flow rate  $Q=10^{-5} \text{ m}^3 \cdot \text{s}^{-1}$ .

Figures 5 and 6 show respectively the velocity fields and the velocity profiles in the two kinds of geometries. The flow velocity stays lower than  $0.2 \text{ m} \cdot \text{s}^{-1}$  and thus the deduced Reynolds number lower than  $10^{-2}$ . It confirms that fluid inertia effects are negligible. Both figures show a zone of stagnation in front of the inlet surface near the area of direction change, where the velocity is very low. The residence time grows extensively and the scorch risk is then

enhanced. But while the general velocity profile in the bifurcation is reduced, the bend zone presents an increase of the maximal velocity of 12 %, caused by the reduction of the flowing diameter during the change of direction. Moreover, the perturbation near the internal corner is clearly visible in the case of the bend zone, while the perturbation is lighter within the bifurcation, where the velocities are strongly reduced. Figure 6 shows that contrary to the straight runner, whose velocity profile remains the same all along the flow, in the bend zone the elastomer flow accelerates and a striction zone appears due to material stagnation in the corner. As a consequence, the velocity profile following the change of direction is shifted. In the bifurcation, the elastomer flow is divided in two equal parts, wherein the velocity profiles are shifted towards the exterior wall. But contrary to the bend zone, the equivalent flowing section is doubled. As a consequence, the velocities are strongly reduced.

The thermal profiles at the outlet of the geometries are presented in Fig. 7. In the straight runner case, viscous heating is concentrated near the wall where the shear rates are the highest. In the case of the bend zone and the bifurcation, the shift of the velocity profiles observed in Fig. 6 results in the redistribution of the part of the material previously located near the wall in the upstream part of both geometries, before the change of direction. Thus, the material's temperature, depending notably of its thermal history, is mainly concentrated in the inner face in the bifurcation case, and is lightly shifted towards the inner surface in the bend zone case.

Several numerical results are presented in Table 3, describing the elastomer flow through the three geometries, for

**Fig. 8** Chemical reaction progress in the bend zone and bifurcation

a constant inlet flow rate  $Q=10^{-5}\text{ m}^3\cdot\text{s}^{-1}$ . In the three configurations, the mean overheating stays lower than 5 °C. Since thermal dependence of viscosity is neglected in the model, a sensitivity analysis was performed and has shown that the involved variation of viscosity, considering Eq. (11), is lower than 10 %.

In the case of the bend zone, the heat generated by viscous dissipation ( $\Phi$ ) is lower than in the straight runner. 70 % is conserved in the bend zone flow, whereas only 68 % is kept in the straight runner case, respectively corresponding to 71 W and 67 W. This difference can be explained by the higher stagnation volume in the bend zone ( $\alpha_s=1.8\%$ ). In the change of flow direction (Fig. 5), the exchanges with the external surface are limited due to the presence of stagnated material, acting as an insulating layer, between the flow and the external surface. Thus, using a bend zone enables to conserve energy generated by viscous dissipation and limits heat losses. The consequence is a saving of 1 °C on outlet temperature and equivalent standard deviation ( $\sigma_T=3.2\text{ °C}$ ).

In spite of a lower pressure variation in the bifurcation, result of the division of the flow, and of a higher heat generated by viscous dissipation in the straight runner, the part of energy exchanged with the external surface remains around 30 %, regardless of the geometry considered. In the bifurcation, material located at the corner of the inner wall is redistributed in the center of the flow after the change of direction (Fig. 6). This material redistribution has two consequences: in the bifurcation, the material temperature is more homogeneous ( $\sigma_T=1.9\text{ °C}$ ), and the outlet bulk temperature, weighted by velocity, is of 1 K higher. Indeed, at the bifurcation outlet, the material is warmer than in other geometries at the center of the flow where the velocity is the highest. However, the inconvenience of bifurcation is to present a more important volume of stagnation ( $\alpha_s=2.4\%$ ).

Figure 8 gives the chemical reaction progress in the bend zone (a) and bifurcation (b) at several positions inside the geometry. These results are obtained thanks to particles tracking (cf §2.3). The first observation is the concentration of particles far from the wall due to stagnation material. The difficulty to send numerically particles in these zones tends to minimize the obtained  $\beta_{out}$  value. This point shall be the subject of a future improvement. However, results also show that the two suggested geometries enable a higher reaction progress to be obtained. Thus, the defined criterion  $I_\beta$ , similar for the bend zone and the bifurcation, express a similar kinetic performance at the outlet.

## Conclusions

The developed model enables to control the influence of the geometry and of the process parameters on viscous

dissipation, velocity field and chemical reaction progress. For the control of the curing state of elastomer in mould during forming process, it is relevant to control the thermal and kinetic behavior of elastomer flow in the runners. The change of geometry is at the origin of a redistribution of the material and also a homogenization of the material temperature and of the reaction progress. Thus, using adapted geometries as flow separator can be useful provided we correctly apprehend the impact of viscous dissipation in the high shear rate zones. The results show that viscous heating represents a non-negligible energy which can be used to reduce the curing time of the moulded part. In view of these results, it should be interesting to predict the material's kinetic behavior with lower extrusion temperatures, where a higher balance between the influences of both residence time and viscous dissipation would take place, in particular at high flow rates. Moreover, a second perspective of this work should be the improvement of the viscosity model, by taken into account thermal dependence or viscoelasticity behavior.

## References

1. Brinkman H (1951) Heat effects in capillary flow I. Appl Sci Res 2:120–124
2. Karkri M, Jarny Y, Mousseau P (2008) Thermal state of an incompressible pseudo-plastic fluid and nusselt number at the interface fluid-die wall. Int J Therm Sci 47:1284–1293
3. Pujos C, Régnier N, Defaye G (2008) Determination of the inlet temperature profile of an extrusion die in unsteady flow. Chem Eng Process 47:456–462
4. Yataghene M, Fayolle F, Legrand J (2009) Experimental and numerical analysis of heat transfer including viscous dissipation in a scraped surface heat exchanger. Chem Eng Process 48:1445–1458
5. Laun H (2003) Pressure dependent viscosity and dissipative heating in capillary rheometry of polymer melts. Rheol Acta 42:295–308
6. Kang SY, Jayaraman K (2002) Wall slip and viscous heating effects on the flow of polypropylene/EP rubber blend in capillary rheometer. J Ind Eng Chem 8:370–374
7. Ha YS, Cho JR, Kim TH, Kim JH (2008) Finite element analysis of rubber extrusion forming process for automobile weather strip. J Mater Process Technol 201:168–173
8. Mani S, Cassagnau P, Bousmina M et al (2009) Cross-linking control of PDMS rubber at high temperatures using TEMPO nitroxide. Macromolecules 42:8460–8467
9. Launay J, Allanic N, Mousseau P, Deterre R (2011) Thermal and kinetic modelling of elastomer flow—application to an extrusion die. In: The 14th international ESAFORM conference on material forming (BELFAST), AIP Conf. Proc. 1353:1101–1106; doi:10.1063/1.3589663
10. Beaumont JP (2007) Runner and gating design handbook, 2nd edn. Hanser, Munich
11. Alok GO, Yuan X-F (2010) Numerical simulation of polymer foaming process in extrusion flow. Chem Eng Sci 65:3749–3761
12. Agassant JF, Avenas P, Sergent JP, Carreau PJ (1991) Polymer processing: principles and modeling. Hanser, Munich
13. Limper A, Schramm D (2002) Process description for the extrusion of rubber compounds—development and evaluation of a screw design software. Macromol Mater Eng 287:824–835



14. Bird RB, Stewart WE, Lightfoot EN (2002) Transport phenomena, 2nd edn. J. Wiley & Sons, Inc
15. Crawford B, Watterson JK, Spedding PL, Raghunathan S, Herron W, Proctor M (2005) Wall slippage with siloxane gum and silicon rubbers. *J Non-Newtonian Fluid* 129:38–45
16. Rafei M, Ghoreishy MHR, Naderi G (2009) Development of an advanced computer simulation technique for the modeling of rubber curing process. *Comp Mater Sci* 47:539–547
17. Claxton NE, Liska JW (1964) Calculation of state of cure in rubber under variable time temperature conditions. *Rubber Age* 9:237–244
18. Isayev A, Deng J (1987) Nonisothermal vulcanization of rubber compounds. *Rubber Chem Technol* 69:277–312
19. Cheheb Z, Mousseau P, Sarda A, Deterre R (2011) Thermal conductivity of rubber compounds versus the state of cure. *Macromol Mater Eng* 297:228–236
20. Gill P, Sauerbrunn S, Reading M (1993) Modulated differential scanning calorimetry. *J Therm Anal Calorim* 40:931–939
21. Arrilaga A, Zaldua AM, Atxurra RM, Farid AS (2007) Techniques used for determining cure kinetics of rubber compounds». *Eur Polymer J* 43:4783–4799
22. Lamnawar K, Mazazouz A (2006) Rheological study of multilayer functionalized polymers: characterization of interdiffusion and reaction at polymer/polymer interface. *Rheol Acta* 45:411–424
23. Ramorino G, Girardi M, Agnelli S, Franceschini A, Baldi F, Vigano F, Ricco T (2010) Injection molding of engineering rubber components: a comparison between experimental results and numerical simulation. *Int J Mater Form* 3:551–554
24. Bagley EB (1957) End corrections in the capillary flow of polyethylene. *J Appl Phys* 28:624–627
25. Rabinowitsch B (1929) Über die viskosität und elastizität von Solen. *Z Phys Chem* 145:1–26, in German
26. Winter HH (1977) Viscous dissipation in shear flows of molten polymers. *Adv Heat Tran* 13:206–267
27. Sombatsompop N, Tan MC, Wood AK (1997) Flow analysis of natural rubber in a capillary rheometer. I: rheological behavior and flow visualization in the barrel. *Polym Eng Sci* 37:270–280
28. Ghoreishy MHR, Razavi-Nouri M, Naderi G (2005) Finite element analysis of a thermoplastic elastomer melt flow in the metering region of a single screw extruder. *Comp Mater Sci* 34:389–396
29. Baaijens FPT (1998) Mixed finite element methods for viscoelastic flow analysis: a review. *J Non-Newtonian Fluid* 79:361–385
30. Connelly RK, Kokini JL (2007) Examination of the mixing ability of single and twin screw mixers using 2D finite element method simulation with particle tracking. *J Food Eng* 79:956–969
31. Wei D, Luo H (2003) Finite element solutions of heat transfer in molten polymer flow in tubes with viscous dissipation. *Int J Heat Mass Transfer* 46:3097–3108